NASA/TM–2020–5004166

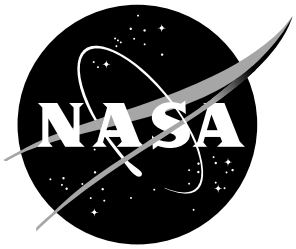

ANC of Radiated Sound from a Small UAS Rotor Using Virtual Error Sensors

Melissa Polen and Christopher Fuller
National Institute of Aerospace, Hampton, Virginia

Noah Schiller
Langley Research Center, Hampton, Virginia

August 2020

NASA STI Program. . . in Profile

Since its founding, NASA has been dedicated to the advancement of aeronautics and space science. The NASA scientific and technical information (STI) program plays a key part in helping NASA maintain this important role.

The NASA STI Program operates under the auspices of the Agency Chief Information Officer. It collects, organizes, provides for archiving, and disseminates NASA's STI. The NASA STI Program provides access to the NASA Aeronautics and Space Database and its public interface, the NASA Technical Report Server, thus providing one of the largest collection of aeronautical and space science STI in the world. Results are published in both non-NASA channels and by NASA in the NASA STI Report Series, which includes the following report types:

- TECHNICAL PUBLICATION. Reports of completed research or a major significant phase of research that present the results of NASA programs and include extensive data or theoretical analysis. Includes compilations of significant scientific and technical data and information deemed to be of continuing reference value. NASA counterpart of peer-reviewed formal professional papers, but having less stringent limitations on manuscript length and extent of graphic presentations.
- TECHNICAL MEMORANDUM. Scientific and technical findings that are preliminary or of specialized interest, e.g., quick release reports, working papers, and bibliographies that contain minimal annotation. Does not contain extensive analysis.
- CONTRACTOR REPORT. Scientific and technical findings by NASA-sponsored contractors and grantees.
- CONFERENCE PUBLICATION. Collected papers from scientific and technical conferences, symposia, seminars, or other meetings sponsored or co-sponsored by NASA.
- SPECIAL PUBLICATION. Scientific, technical, or historical information from NASA programs, projects, and missions, often concerned with subjects having substantial public interest.
- TECHNICAL TRANSLATION. English-language translations of foreign scientific and technical material pertinent to NASA's mission.

Specialized services also include organizing and publishing research results, distributing specialized research announcements and feeds, providing information desk and personal search support, and enabling data exchange services.

For more information about the NASA STI Program, see the following:

- Access the NASA STI program home page at `http://www.sti.nasa.gov`
- E-mail your question to `help@sti.nasa.gov`
- Phone the NASA STI Information Desk at 757-864-9658
- Write to:
  NASA STI Information Desk
  Mail Stop 148
  NASA Langley Research Center
  Hampton, VA 23681-2199

NASA/TM–2020–5004166

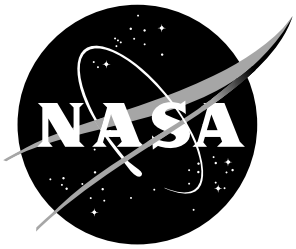

ANC of Radiated Sound from a Small UAS Rotor Using Virtual Error Sensors

Melissa Polen and Christopher Fuller
National Institute of Aerospace, Hampton, Virginia

Noah Schiller
Langley Research Center, Hampton, Virginia

National Aeronautics and
Space Administration

Langley Research Center
Hampton, Virginia 23681-2199

August 2020

Acknowledgments

The authors would like to thank Nikolas Zawodny for his assistance with the test setup and for many helpful discussions regarding rotor noise.

Available from:

NASA STI Program / Mail Stop 148
NASA Langley Research Center
Hampton, VA 23681-2199
Fax: 757-864-6500

Abstract

Small unmanned aerial systems (UAS) are becoming increasingly common for private, military, and commercial use, increasing community noise exposure. Reducing the noise produced by UAS could help improve community acceptance. Active noise control (ANC) might be used to attenuate noise produced by UAS, however, traditional ANC systems require a physical sensor in the far-field, which is not feasible. This paper assesses a virtual error sensing (VES) method that eliminates the need for a far-field sensor. This paper describes the proposed VES strategy, and presents numerical simulations and experimental results that highlight the benefits and limitations of the approach. Results for the VES system alone and with an ANC approach are presented and discussed. Experimental testing focused on attenuating the tonal noise produced by one 2-bladed rotor with a tip radius of 11.9 cm. Pressure variations caused by blade rotation were measured in the near and far-field using electret microphones and externally polarized condenser microphones, respectively. The filtered-x least mean squares algorithm was used in conjunction with the VES system to attenuate the far-field response. Experimental results show reductions between 6-13 dB at varying far-field locations and rotation rates.

Contents

1 Introduction

Community noise concerns could ultimately limit the use of small unmanned aerial systems (UAS) if low-noise designs and technologies are not available. Recent human response tests by Christian and Cabell [1] have shown that sounds produced by small UAS are more annoying than similar amplitude sounds produced by cars and trucks. In other words, small UAS may need to be quieter than conventional road vehicles. This finding reinforces the need for small UAS noise research.

To help facilitate low-noise designs, several researchers [2–4] have characterized the noise of small UAS components, subsystems, and vehicles. They have shown that the noise has a strong tonal component, with well-defined peaks at the blade passage frequency (BPF) and its harmonics. Broadband noise can also be important above 1 kHz, however, the rotor tones tend to dominate at lower frequencies [5, 6]. Insights gained from these studies may lead to quieter designs, but noise control technologies will still be needed for some applications.

Passive noise control technologies can be used to mitigate the impact of small UAS operations. For example, there are commercially available shrouds [7] that may be able to modify the source directivity and reduce noise at certain locations around the vehicle. Active noise control (ANC) has also been considered for small UAS vehicles. These will primarily be effective in mid to high frequency ranges. ANC systems typically consist of an error sensor (i.e., microphone), a controller, and a loudspeaker, which are used to cancel the noise produced by UAS rotors in specific regions around the vehicle. Previous tests by Schiller and Zawodny [8] have demonstrated that it is possible to actively reduce low-frequency tonal noise generated by a small UAS rotor by over 30 dB in specific directions. The ANC system used in that study, however, relied on a physical sensor in the far field,

close to 2 m from the rotor, which is not feasible in flight. In related work, Thomas et al. [9] experimentally studied the use of a ring of active sources and error sensors located in a turbo fan inlet to actively control radiated tonal fan noise.

The purpose of this study is to evaluate the performance of an ANC system with a virtual error sensor that estimates the far-field acoustic response based on measurements of sound on the vehicle, in the near-field of the rotor. This paper starts with a description of the proposed ANC system and virtual sensing strategy. The experimental setup is then presented, followed by details of the real-time control system. A numerical model is then described, which is used to visualize the spatial extent of sound pressure level (SPL) attenuation while applying ANC using a virtual sensor. Finally, results are presented comparing the SPL achieved at a far-field location after applying ANC with a virtual sensor, as well as the SPL attenuation achieved at surrounding far-field locations.

2 Active Noise Control using Virtual Error Sensing

A standard feedforward ANC system, as implemented by Schiller and Zawodny [8] and described by Fuller et al. [10] for example, is depicted in Fig. 1a. This system uses a microphone to measure the sound produced by the rotor at some location in the geometric far-field (away from the rotor). This is referred to as the error signal. A tachometer provides a reference signal that is correlated with the noise generated by the rotor. The error and reference signals are then passed through an adaptive digital controller, which produces a control signal that is fed to the loudspeaker. If everything is configured correctly, the sound produced by the loudspeaker will be out-of-phase with the noise from the rotor at the far-field microphone, resulting in significant attenuation of the noise in a region surrounding the microphone.

The focus of this paper is on the configuration shown in Fig. 1b. In this case, the feedforward control system includes a virtual error sensing method. Rather than using a physical microphone at the desired far-field location to provide the error signal, the signal is estimated based on the response of a near-field sensor that is close to the rotor. The estimated error and response signals are then passed through the controller to generate the control input. The error signal is estimated using the near-field sensor, the control signal, and previously identified relationships determined during initial system identification tests. As in Fig. 1a, the aim of a control system that uses a virtual sensor is to generate a control signal for the loudspeaker that will reduce the noise at a desired far-field location without any physical far-field microphones being present.

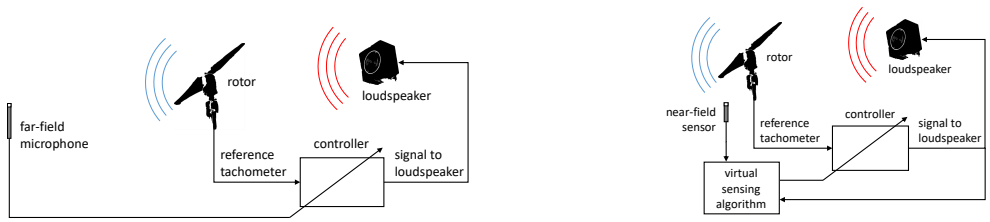

(a) (b)

Figure 1: Feedfoward control approach using: (a) standard ANC system, or (b) ANC system with virtual error sensing.

The filtered-x least-mean-square algorithm (FxLMS) was used in this study. The algorithm is commonly used in ANC applications due to its simplicity and efficiency. The FxLMS algorithm adapts the LMS algorithm to account for the path from the loudspeaker to the far-field microphone, $\hat{G}_{vu}$. Figure 2 illustrates how the reference signal, $x(n)$ and error signal $e(n)$ are used to update the controller $W(z)$ and generate the control input, $u(n)$.

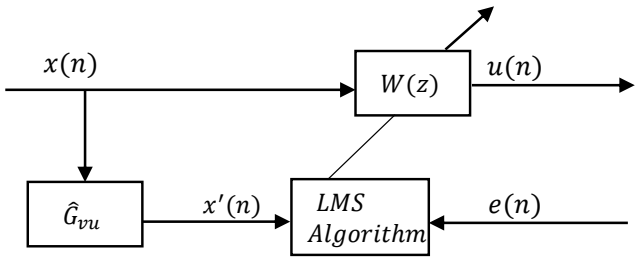

Figure 2: Block diagram of feedforward control using the FxLMS algorithm.

The virtual microphone arrangement (VMA), developed by Elliott and David [11], was one of the first virtual sensing techniques applied to an ANC system. The VMA assumes that the sound pressure due to the primary source (e.g., the rotor) at the physical microphone and the virtual microphone locations are equal. The field due to the secondary source (i.e., the loudspeaker) is not assumed to be equal at the two locations. Transfer functions between the control signal and the physical microphone, $\hat{G}_{pu}$, and between the control signal and the virtual location are created during a preliminary identification step. The combined response (i.e., due to both the primary and secondary sound fields) at the virtual location is estimated based on the control signal, the transfer functions, and the measured response at the physical sensor, $p_t(n)$, as

$$\hat{e}(n) = p_t(n) + [\hat{G}_{vu} - \hat{G}_{pu}]u(n) \tag{1}$$

This virtual sensing approach has been used successfully in applications where the distance between the physical microphone and virtual location is small, like an active head-

rest [12]. However, the underlying assumptions break down when the physical microphone is not close, compared to the acoustic wavelength of the primary disturbance, to the location where attenuation is desired. The VMA is not appropriate for the small UAS application, since the goal is to reduce the noise in the far-field using physical error sensors on the vehicle.

The remote microphone technique [13] (RMT), as depicted in Fig. 3, was the virtual sensing method considered in this study. The RMT is an extension of the VMA that accounts for differences in the primary sound field between the physical microphone and virtual microphone locations using an observation filter (OF) identified during a preliminary identification step. Spatial differences in the sound field can be attributed to acoustic propagation, reflections, diffraction, source directivity effects, etc. The OF captures the linear relationship between the near-field sensor and the far-field microphone. For ANC applications, the filter is constrained to be causal, and therefore, the RMT is generally best suited for tonal sources. Similar to the VMA, the transfer functions from the control signal to the near-field sensor, $\hat{G}_{pu}$, and from the control signal to the far-field (virtual location), $\hat{G}_{vu}$, are also estimated during the preliminary identification step. The transfer functions relating to the far-field use temporarily placed far-field microphones to identify the paths. The pressure in the near-field due to the rotor is calculated as

$$\hat{p}_r(n) = p_t(n) - \hat{p}_u(n) \tag{2}$$

where p_t is the total measured near-field response and $\hat{p}_u$ is the near-field response due to the loudspeaker, which leads to

$$\hat{p}_r(n) = p_t(n) - \hat{G}_{pu}u(n) \tag{3}$$

using the transfer function $\hat{G}_{pu}$ and the loudspeaker signal, u. The pressure response due to the rotor at the far-field (i.e., virtual error sensor) location is determined by the equation

$$\hat{v}_r(n) = OF\hat{p}_r(n). \tag{4}$$

The estimated far-field response is

$$\hat{e}(n) = \hat{v}_r(n) + \hat{v}_u(n) \tag{5}$$

where $\hat{v}_u$ is the far-field response due to the loudspeaker, defined as

$$\hat{v}_u(n) = \hat{G}_{vu}u(n). \tag{6}$$

The complete equation to estimate the far-field response due to the rotor and loudspeaker is

$$\hat{e}(n) = OF[p_t - \hat{G}_{pu}u(n)] + \hat{G}_{vu}u(n), \tag{7}$$

which uses the transfer functions, the near-field measurement, and the loudspeaker signal.

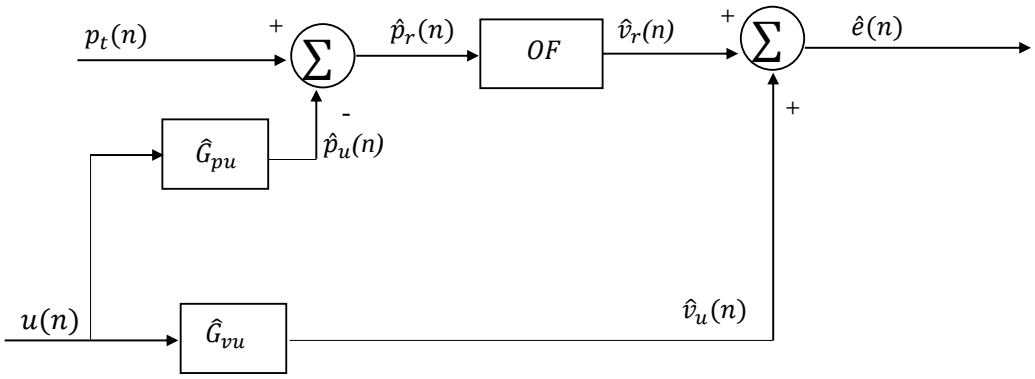

Figure 3: Block diagram of the remote microphone technique.

The remote microphone technique can then be combined with the ANC system, as shown in Fig. 4. A reference signal is provided to the control system, and a near-field sensor measures the total pressure response caused by both the rotor and the loudspeaker. The control signal is used with the transfer functions $\hat{G}_{pu}$ and $\hat{G}_{vu}$ to estimate the far-field pressure response, which is subsequently passed through the controller.

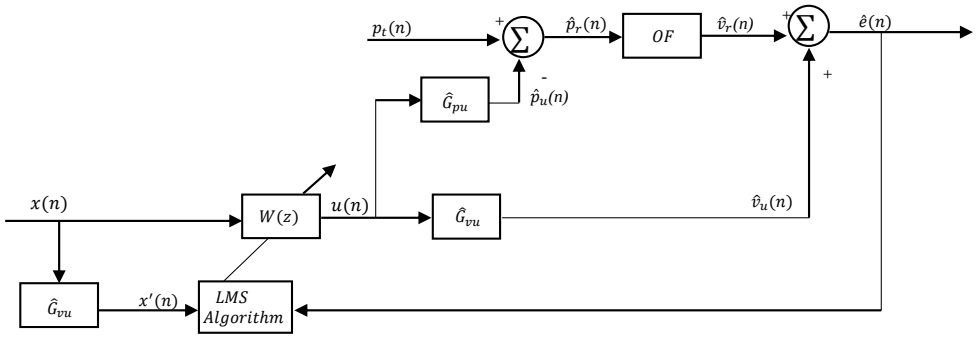

Figure 4: Block diagram of the digital controller with a virtual error sensor.

3 Experimental Setup

Experimental testing was conducted in the NASA Langley Structural Acoustic Loads and Transmission (SALT) anechoic chamber. Foam wedges that are 0.914 m tall line the walls, ceiling, and floor to create a nearly anechoic environment down to 100 Hz. Tests were conducted using a single rotor with two-blades with a tip radius of 11.9 cm, which was secured to a test stand located in the center of the chamber, as shown in Fig. 5a. Similar to Zawodny and Boyd [3], a 3D printed cone with a minor and major diameter of 20 mm and 70 mm, respectively, and length of 163 mm was positioned below the rotor to mimic an airframe. Electret microphones were embedded into the cone to measure the near-field pressure response. This study used the electret directly under the rotor tip to establish the virtual error sensor. A five microphone array located 1.905 meters from the rotor test stand captured the far-field acoustic pressure response. A 7.6 cm diameter loudspeaker was positioned 8.9 cm

below the plane of the rotor and was offset 17.8 cm from the center of the rotor (away from the microphone array). Additionally, the speaker center was offset 14 cm to the left of the microphone array. Figure 5b shows the near-field configuration. The rotor was primarily operated at 5250 RPM, which was measured and verified using an optical tachometer. Microphones 1, 3, and 5 were chosen as targeted locations of control, and microphones 2 and 4 provided supplementary far-field pressure responses to estimate the global nature of the active attenuation.

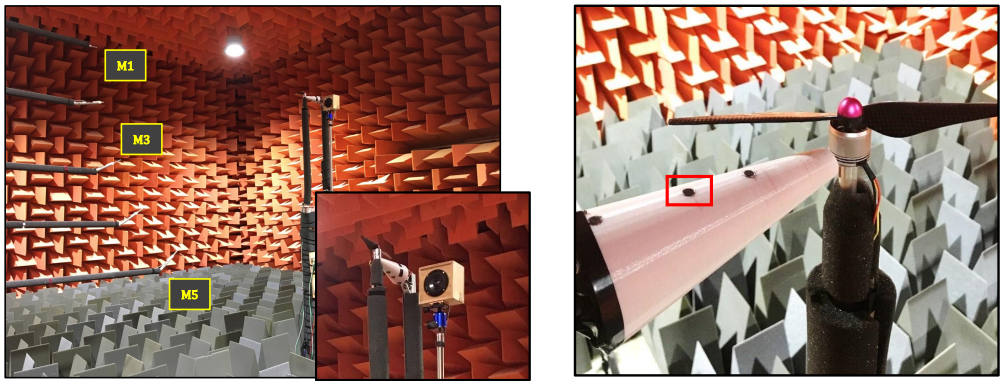

(a) (b)

Figure 5: Test setup showing (a) the rotor configuration relative to the microphone array, and (b) the electrets embedded in the cone, with the electret used in this study outlined in red.

4 Real-Time Control

The control system was implemented using a Speedgoat Real-Time target machine I/O 104 board. Low-pass antialiasing and reconstruction filters with a cutoff frequency of 1500 Hz were used on both the inputs and outputs of the digital controller. It should be noted that two computer systems were used during this test; one to implement real-time control and one for data acquisition. The real-time control system's sampling rate was 5000 Hz. The data acquisition system's sampling rate was 50 kHz with an acquisition time of 20 seconds. The rotor speed was specified on the data acquisition computer. Data acquisition began when the rotor speed converged to the desired rotation speed. Once the data set was collected, the rotor speed was zeroed and the air in the chamber was allowed to settle for 20 seconds before the next data set was collected. Data sets during which no control input was applied are referred to as open-loop; closed-loop data sets refer to those during which ANC was turned on. Closed-loop data sets were collected as follows: the rotor was turned on and allowed to converge to the set speed, then the control system was enabled and the adaptive filter was allowed to converge. Once the control system was converged, data acquisition began. After the acquisition period of 20 seconds, the rotor and control system were turned off. The control filters used in this study contained 1024 coefficients. A bandpass filter from 50-425 Hz was applied to the reference signal and near-field signal signal during the system ID as well as open and closed-loop data collection to reduce the amplitude of the

DC offset and higher harmonic content, as this study aimed to attenuate the SPL at only the first few rotor harmonics. Additionally, a high-pass filter was applied to the temporarily placed far-field microphone, to reduce the amplitude of the DC offset.

In order to apply ANC using a virtual error sensor through the RMT, three paths must be identified: an observation filter (OF) between the near-field and the far-field transducers due to the rotor noise, the plant $\hat{G}_{pu}$ from the speaker to the near-field sensor, and the plant $\hat{G}_{vu}$ from the speaker to the far-field microphone. This estimation is referred to as system identification. The OF was estimated by measuring the pressure response at the electret and the far-field microphones due to the rotor. The OF depends on rotor speed; for most of the tests described here the rotor was set to 5250 RPM. Once pressure response data were collected, the optimal 1024-point FIR filter representation of the path between the two transducers was determined using a Wiener filter solution technique [14] . The paths $\hat{G}_{pu}$ and $\hat{G}_{vu}$ estimate the relationship between the control speaker and near-field electret and the far-field microphone, respectively. The path estimates included the effects of the system's physical components: the antialiasing filters, the bandpass filter, the ADC/DAC, amplifier, speaker, electret, and far-field microphone. After the control speaker outputted band limited white noise and the near-field and far-field responses were collected, the optimal filter coefficients were calculated using the Wiener filter

$$\mathbf{w}_{opt} = \mathbf{A}^{-1}\mathbf{b} \tag{8}$$

where **A** is the autocorrelation matrix of the input, which is the speaker input in this application, and **b** is the cross-correlation vector between the speaker and the electret or microphone. Each system identification collected data for 10 seconds and was split into two data sets that were each 5 seconds long. The first data set was passed through the Wiener filter to estimate the optimal filter coefficients. The second data set served as a validation set, which compared the estimated far-field response to the measured far-field response.

5 Numerical Model

Prior to experimental testing, an acoustic finite element model (FEM) was used to predict the spatial extent of the attenuation. Specifically, the model predicted the SPL around the rotor at the blade passage frequency with and without the active loudspeaker turned on. Attenuation was then determined by comparing the difference in the predicted levels. For the closed-loop predictions, the magnitude and phase of the monopole source, representing the loudspeaker, were determined using the virtual sensing approach and system identification procedures previously described.

The model configuration simulated the setup used in experimental testing. The model consisted of a ring source that represented the rotor, a monopole representing the loudspeaker, a rigid conical airframe, microphones in the near- and far-field, and a hemisphere defining the surrounding domain. A perfectly matched layer (PML) was included around the outer perimeter of the hemisphere to simulate an anechoic environment. The location of the microphones in the near- and far-field were consistent with that of the electrets and

microphone array used in testing. The loudspeaker was modeled using a constant pressure monopole point source and the UAS airframe was modeled as a cone, matching the test setup. Figure 6 shows the arrangement of the far-field point microphones and near-field configuration.

The rotor source, which approximates rotor thickness noise, as discussed by Chapman [15] and Prentice [16], was described using the equation

$$h = S_m e^{-imB\theta} \tag{9}$$

where m is the harmonic number, B is the rotor blade count, and θ is the azimuthal angle. The variable S_m is a constant source term. Although Eq. 9 does not account for the loading noise, the directivity predicted by the model is helpful in understanding the locations of reduction and amplification during ANC.

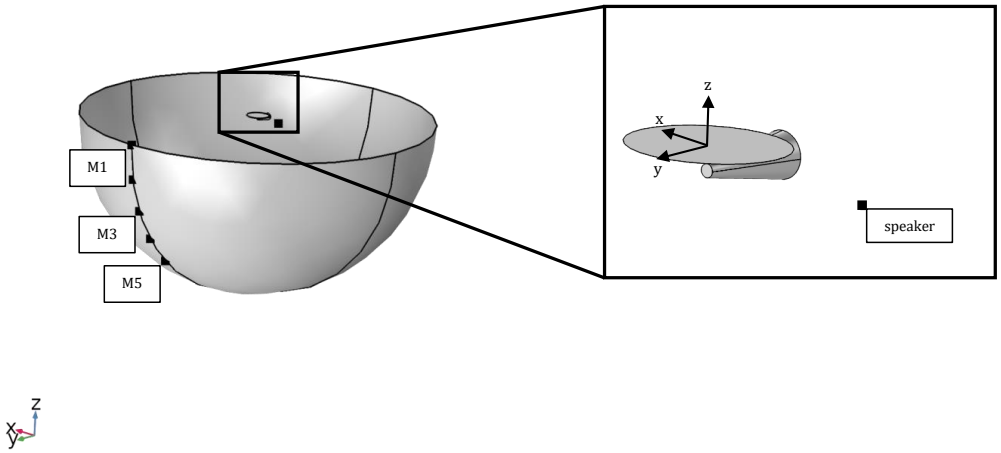

Figure 6: Numerical model of the test setup.

6 Results

The results are divided into three sections. The first discusses the performance of the virtual error sensor, which is assessed by comparing the measured far-field SPL to the response estimated using the observation filter. The second portion presents and compares ANC attenuation results using a virtual error sensor at multiple microphone locations. The spatial extent of attenuation is also shown by observing the change in SPL at surrounding microphone locations apart from those used during the system ID, which are compared to numerical predictions. Finally, the robustness of an observation filter is explored by comparing the SPL attenuation at multiple rotor speeds using an OF identified at a single rotation rate.

The feedforward ANC system considered in this paper is fundamentally limited to tonal noise, as the optical tachometer that provides the reference signal is only correlated with

tonal noise (BPF and harmonics). This limitation means that the virtual error sensor only needs to provide an accurate estimate of the far-field response at the corresponding tones, which also eliminates causality concerns. As shown in Fig. 3, the virtual sensing strategy requires three models to estimate the far-field response using the near-field measurement. The first is the observation filter (OF) that describes the relationship between the far-field microphone and near-field electret due to the rotor. The remaining plants $\hat{G}_{pu}$ and $\hat{G}_{vu}$ describe the relationship from the loudspeaker to the electret and from the loudspeaker to the far-field microphone, respectively. While the accuracy of each model is important, the OF is the most challenging to estimate since it is sensitive to the rotor operating conditions.

6.1 Virtual Error System Experimental Results

One way to assess the accuracy of the OF is to compare the far-field estimate and the measured response with control off. When the system is open loop and the control signal is zero, the far-field estimate is generated by filtering the near-field signal by the observation filter. Figure 7 compares the measured and estimated far-field SPL at M3 for the open loop system. In this case, the test was conducted with the rotor at 5250 RPM, which also corresponds to the rotation rate used to produce the OF. The coherence between the reference signal and the estimated far-field pressure is also shown for comparison. To avoid control spillover [10, 17], an accurate estimate of the far-field response is needed at frequencies where the coherence is high. Coherence is above 0.8 at the highlighted BPF and harmonics, suggesting that the virtual sensor needs to be accurate at these frequencies. The estimated and measured SPLs at the highlighted BPF and harmonics match within 1 dB of each other from the shaft rotation rate to 700 Hz, indicating that the OF can estimate the rotor response at the far-field virtual location over this frequency range. Although the bandpass filter was applied to the near-field and reference signals while performing the system ID, the highpass filter on the temporarily placed far-field microphone allowed for frequencies outside of the bandpass filter range to be estimated. Further, the mean-square-error (MSE) between the measured and estimated magnitude and phase OF values at each of the frequencies highlighted in Fig. 7, normalized with the mean-square measured values is 0.022 and 0.025, respectively. Values close to 0 indicate low error between the measured and estimated OF relative to the measured OF, while larger values indicate high normalized error.

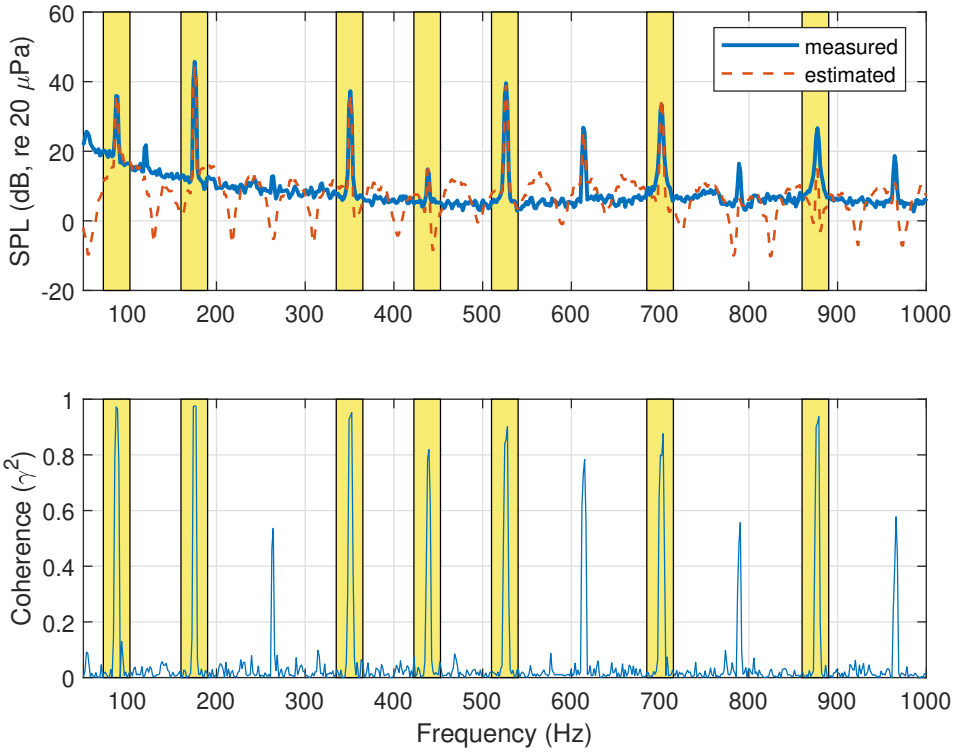

Figure 7: Comparison of the measured (blue) and estimated (red) far-field response at M3 caused by the rotor operating at 5250 RPM is shown in the upper plot. The coherence between the reference signal and estimated far-field response is shown in the lower plot.

6.2 Measured Active Control Performance with Virtual Error Sensors

Figure 8a compares the closed-loop results using the virtual error sensor (targeting M1) with the open-loop response at M1. At the targeted microphone, the SPL is attenuated by 13 dB at the shaft harmonic, 87.5 Hz, and by 9 dB at the rotor BPF, 175 Hz. The SPL of the fourth shaft harmonic, 350 Hz, is also significantly attenuated by about 6 dB. However, the SPL of the third and fifth shaft harmonics, 262.5 and 437.5 Hz, are amplified by about 3 dB, which could be due to inaccuracies in the OF. The SPL of frequencies greater than 425 Hz are not attenuated due to the bandpass filter that was applied to the near-field and reference sensors. In general, the SPL of the higher harmonics are not changed. Figure 8b provides a similar comparison for microphone M3. In this case, the virtual error sensor was designed to target microphone M3. The SPL at the shaft harmonic and rotor BPF are attenuated by about 5 and 10 dB, respectively. The SPL of the fourth shaft harmonic is also reduced by 2 dB. While the higher harmonics are not amplified, the tone at 262.5 Hz is amplified by almost 10 dB. Again, amplification at this frequency may be due to the errors in the OF, as seen in Fig. 7. Although the SPL at 262.5 Hz is amplified, the overall SPL (OASPL) of M3 during the closed-loop test is reduced by 2.5 dB over the frequency range of 50-5000 Hz, which contains most of the spectral content.

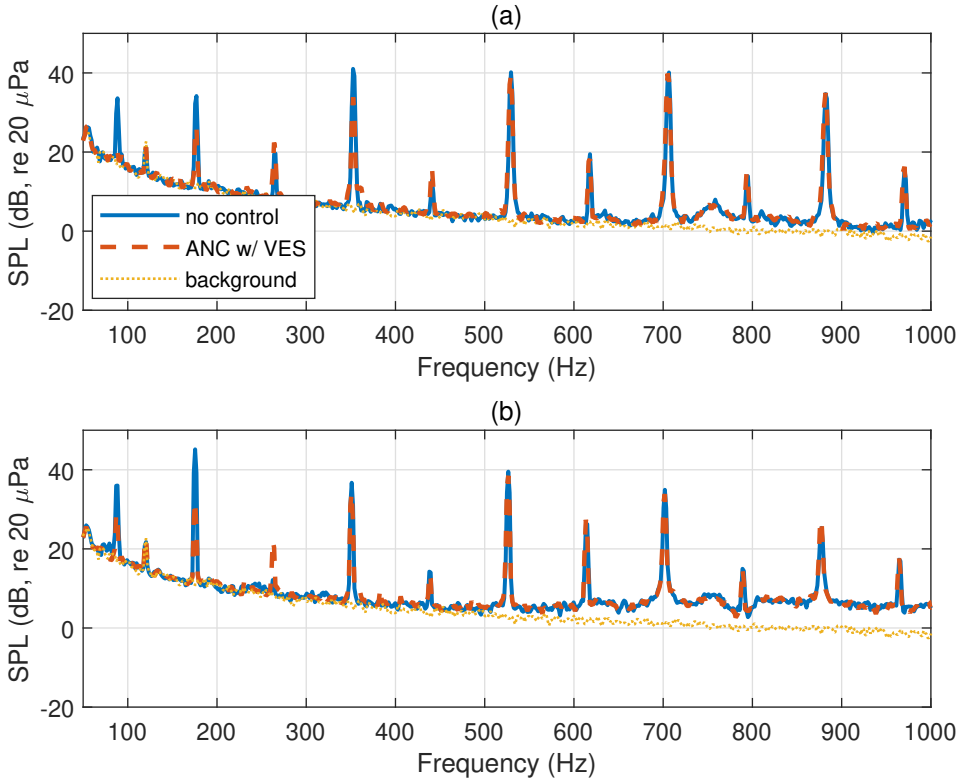

Figure 8: Open-loop SPL (solid blue) compared to closed-loop SPL (dashed red) at the targeted microphone using a virtual error sensor (VES) targeting (a) M1 or (b) M3.

In addition to measuring the far-field SPL at the targeted microphone, the spatial extent of attenuation is also examined by comparing the change in SPL at five far-field microphone locations during open and closed-loop data collection. Figure 9 shows the change in SPL at each microphone using an ANC system designed to minimize the estimated far-field pressure at M1. The SPL at all five microphones is attenuated at the shaft rotation rate, 87.5 Hz, and at the BPF, 175 Hz. At these tones, the SPL at M1 is attenuated most, and M5 is attenuated least, as expected. Although each microphone measures the SPL of a different elevation angle, they share the same azimuthal angle, so Fig. 9a does not necessarily indicate that the ANC system achieves global attenuation at these frequencies. At 350 Hz, the second harmonic of the BPF, M1 and M2 are attenuated while M3, M4, and M5 are amplified. The SPL at odd multiples of the shaft rotation rate, 262.5 and 437.5 Hz, are consistently amplified, which could be due to inaccuracies in the OF. However, amplified levels at these frequencies are still below the dominant tones at the BPF harmonics, as shown in Fig. 8a for example. The tonal variations above 500 Hz are modest, as expected given the bandpass filter on the near-field and reference signals. These small changes might be due test variability introduced by recirculation, for example, which could be assessed in a follow-on study. Figure 9b shows the change in the tonal SPL using an ANC system designed to minimize the estimated far-field pressure at M3 instead of M1. At the shaft rotation rate and rotor BPF, the tonal attenuation is good near M3, however, there is amplification near the edges of the array at M1 and M5. As shown in Fig. 8b, the SPL at the third

multiple of the rotation rate, 262.5 Hz, is significantly amplified at M3, again, potentially due to errors in the OF. Similar to Fig. 9a, the changes in the tonal levels above 500 Hz are small. Consistent trends were also observed when the targeted microphone was M5.

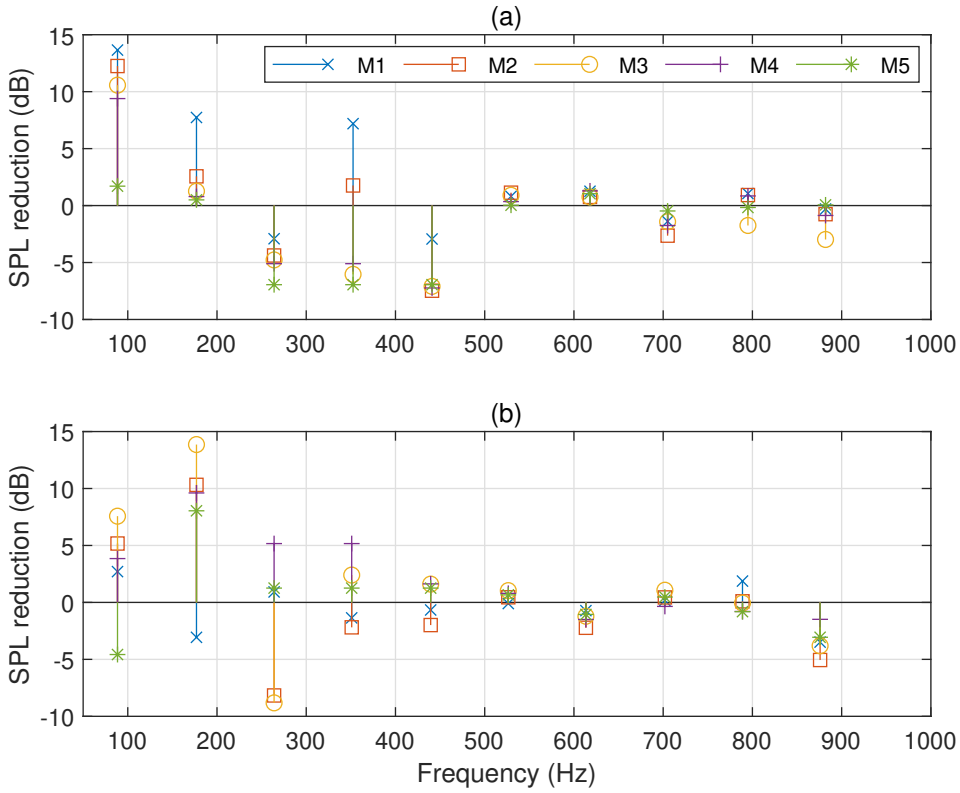

Figure 9: Change in the tonal SPL at the far-field microphones using ANC with a virtual error sensor targeting (a) M1 or (b) M3.

6.3 Numerical Prediction of Active Cancellation

The spatial extent of the quiet zone can be visualized using the numerical model, which was developed to predict the SPL at the BPF in a hemispherical region around the rotor. Figure 10a shows the predicted tonal attenuation using an ANC system designed to minimize the estimated response at M1. Similarly, Fig. 10b shows the tonal attenuation using an ANC system designed to minimize the estimated response at M3. In both cases, significant attenuation is achieved near the targeted microphone, with less attenuation away from that location. The same general trend is observed in Fig. 9. Locations further from the targeted microphone experience less SPL attenuation than locations in close proximity due to the difference in radiation characteristics between the rotor and the loudspeaker [18].

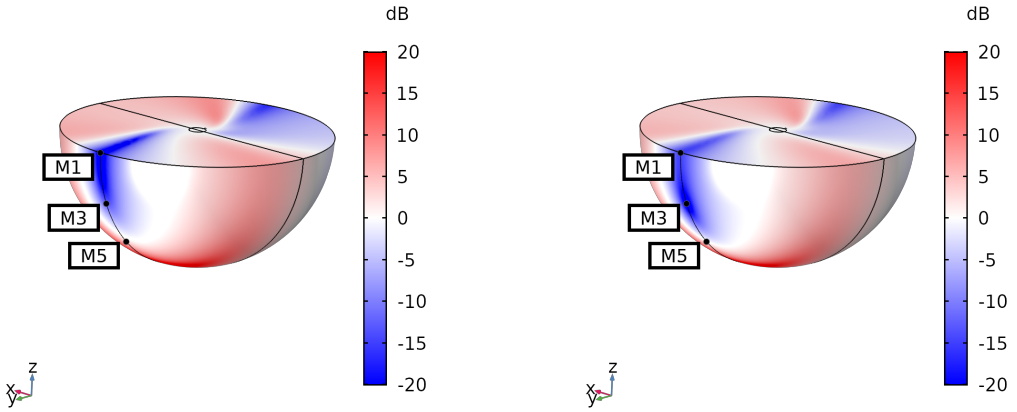

(a) (b)

Figure 10: Numerical predictions showing the change in SPL at 175 Hz using ANC with a virtual sensor targeting (a) M1 or (b) M3.

The OF is at least weakly dependent on rotor speed, in part due to differences in the near-field pressure response caused by the rotor cone interaction. While different OFs could be identified to account for the operating condition of the vehicle, it is important to understand how robust the model is to variations in the rotation rate. The black curves in Fig. 11 show the magnitude and phase of the OF generated with the rotor at 5250 RPM. Magnitude and phase estimates from measured data are also shown with markers. The location of the markers corresponds to the shaft harmonics for three rotation rates. Differences between the black circles (corresponding to 5250 RPM) and the curve imply that even at a fixed rotation rate, the OF is not accurate at all harmonics, particularly odd shaft order harmonics. While the other markers do not fall exactly on the 5250 RPM curve, the agreement is generally good at frequencies below 400 Hz, which implies that a single OF filter may be adequate for a range of rotor speeds. Higher frequencies show significant differences in the magnitude and phase response, which could lead to closed-loop amplification. This supports the experimental results discussed previously.

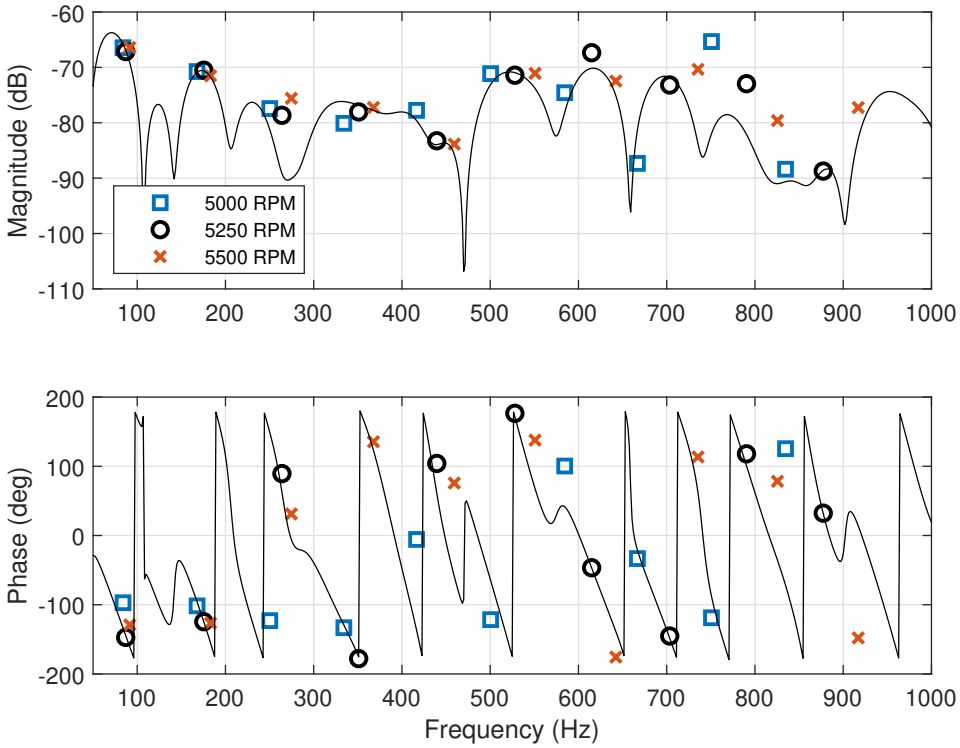

Figure 11: Comparison of the magnitude and phase response for the OF (identified at 5250 Hz) with magnitude and phase estimates from measured data at three rotation rates.

Figure 12 shows the measured tonal attenuation at M3 with three different rotation rates. A single observation filter, generated with the rotor operating at 5250 RPM, was used for all three tests. While performance is best at 5250 RPM, the control system still attenuates the tonal level at the shaft rotation rate and the rotor BPF at the other rotation rates. As discussed previously, the amplification at around 260 Hz is likely due to errors in the observation filter.

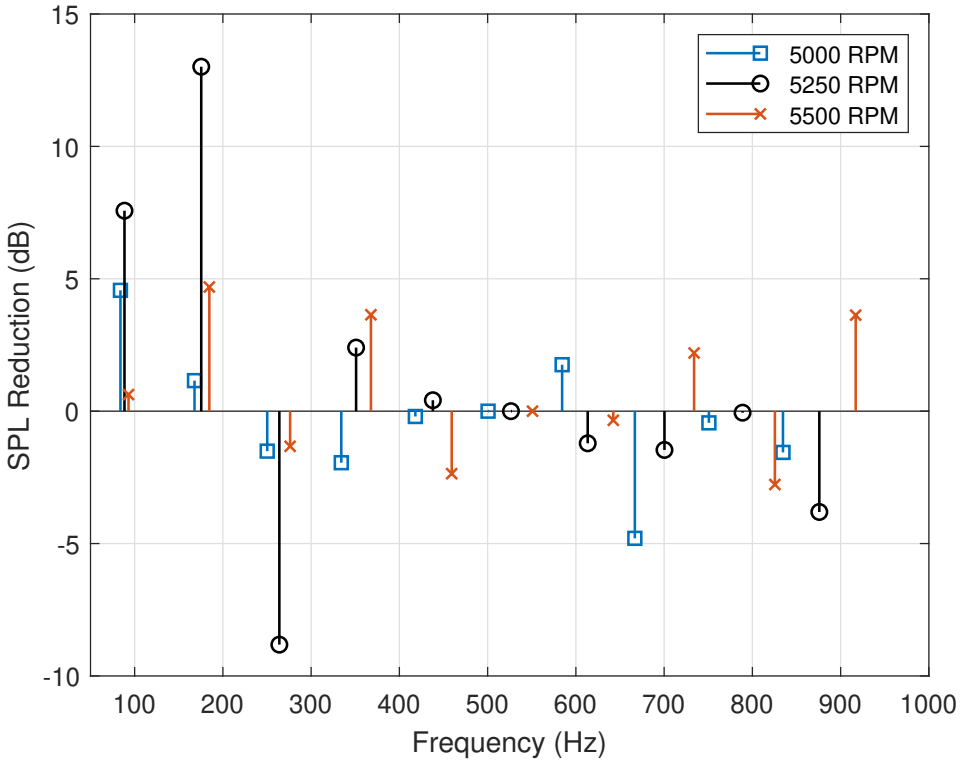

Figure 12: Change in the tonal SPL at M3 when a fixed OF (identified at 5250 RPM) is used at different rotation rates.

7 Concluding Remarks

This paper assesses a virtual error sensing strategy that eliminates the need for a far-field microphone as part of an ANC system applied to UAS rotor noise. The virtual sensor was used to estimate the far-field response at the BPF and other low-order harmonics of the shaft rotation rate, and estimated the BPF and harmonics to be within 1 dB of the measured far-field response up to 700 Hz. Tonal reductions of 6-13 dB were measured experimentally. The spatial extent of the tonal attenuation was also experimentally assessed and compared with predictions. Both measurements and predictions show significant low frequency attenuation near the targeted microphone, accompanied by amplification away from the microphone. The numerical model predicted that the spatial extent of attenuation was consistent with experimental results at a single azimuthal angle. The robustness of the observation filter, used in the virtual error sensor, was evaluated. Based on the results, it appears that a single filter could be sufficient for a limited range of rotor speeds.

In the future, it would be useful to investigate the effect that a multiple input single output (MISO) system has on the performance of the ANC system, using multiple near-field sensors located on the airframe to provide the inputs. Further, the MISO system could be extended to a multiple input multiple output (MIMO) system by using multiple loudspeakers to provide the system outputs. Additionally, future studies might benefit from far-field

microphones at different azimuthal angles to better understand azimuthal changes in the sound field. Future work could also be performed using a smaller loudspeaker that is compact enough to be mounted onto a UAS airframe. The numerical model could also be used to investigate the physics of the ANC approach and optimize its configuration. Lastly, future work could include a more rigorous study of the observation filter, to better define the range of operating speeds that can be used with a single filter.

References

1. A. Christian and R. Cabell. Initial Investigation into the Psychoacoustic Properties of Small Unmanned Aerial System Noise. In *23rd AIAA/CEAS Aeroacoustics Conference*, Denver, CO, June 2017.

2. N. S. Zawodny, D. D. Boyd Jr., and C. L. Burley. Acoustic characterization and prediction of representative, small-scale rotary-wing unmanned aircraft system components. *Proceedings of the AHS 72nd Annual Forum*, May 2016.

3. N. S. Zawodny and D. D. Boyd Jr. Investigation of rotor-airframe interaction noise associated with small-scale rotary-wing unmanned aircraft systems. *Journal of the American Helicopter Society*, pages 1–17, January 2020.

4. N. Intaratep, W. N. Alexander, W. J. Devenport, S. M. Grace, and A. Dropkin. Experimental study of quadcopter acoustics and performance at static thrust conditions. *Proceedings of the 22nd AIAA/CEAS Aeroacoustics Conference*, May 2016.

5. J. Stephenson, D. Weitsman, and N. Zawodny. Effects of flow recirculation on unmanned aircraft system (uas) acoustic measurements in anechoic chambers. *The Journal of the Acoustical Society of America*, 145(3):1153–1155, 2019.

6. N. Zawodny and N. Pettingill. Acoustic wind tunnel measurements of a quadcopter in hover and forward flight conditions. *Proceedings of InterNoise*, 2018.

7. G. Beckermann, I. Hosie, A. Clarke, M. Rowe, S. Rowe, S. Pentecost, and S. Edlin. Sound attenuating performance of nanofibre materials used in unmanned aerial vehicles. *TechConnect Briefs*, 1:212–215, 2018.

8. N.H. Schiller and N. S. Zawodny. Initial developments toward an active noise control system for small unmanned aerial systems. *Proceedings of InterNoise*, August 2018.

9. R. H. Thomas, R. A. Burdisso, C. R. Fuller, and W. F. O'Brien. Preliminary experiment on active noise control of fan noise from a turbofan engine. *Journal of Sound and Vibration*, pages 532–537, March 1993.

10. C. Fuller, S. Elliott, and P. Nelson. *Active Control of Vibration*. Academic Press, London, 1996.

11. S. Elliott and A. David. A virtual microphons arrangement for local active sound control. In *Proceedings of the 1st International Conference on Motion and Vibration Control*, pages 1027–1031, Yokohama, Japan, 1992.

12. J. Garcia-Bonito, S. Elliott, and C. Boucher. Generation of zones of quiet using a virtual microphone arrangement. *The Journal of the Acoustical Society of America*, 101:3498, 1997.

13. A. Roure and A. Albarrazin. The remote microphone technique for active noise control. In *Internoise and Noise-Con Congress and Conference Proceeding*, pages 1233–1244, 1999.

14. S. Elliott. *Signal Processing for Active Control*. Academic Press, 2001.

15. C. J. Chapman. The structure of rotating sound fields. *Proceedings of the Royal Society of London, Series A: Mathematical and Physical Sciences*, 440, 1993.

16. P.R. Prentice. The acoustic ring source and its application to propeller acoustics. *Proceedings of the Royal Society of London, Series A: Mathematical and Physical Sciences*, 437, 1992.

17. M. Balas. Feedback control of flexible systems. *IEEE Transactions on Automatic Control*, 23(4):673–679, 1978.

18. S. Elliott and J. Cheer. Modeling local active sound control with remote sensors in spatially random pressure fields. *The Journal of the Acoustical Society of America*, 137:1936, 2015.

REPORT DOCUMENTATION PAGE

Form Approved
OMB No. 0704–0188

1. REPORT DATE *(DD-MM-YYYY)*	2. REPORT TYPE	3. DATES COVERED *(From - To)*
01-08-2020	Technical Memorandum	1/2018–8/2020

4. TITLE AND SUBTITLE
ANC of Radiated Sound from a Small UAS Rotor Using Virtual Error Sensors

5a. CONTRACT NUMBER
NNL09AA00A

5b. GRANT NUMBER

5c. PROGRAM ELEMENT NUMBER

6. AUTHOR(S)
Melissa Polen and Noah Schiller and Christopher Fuller

5d. PROJECT NUMBER

5e. TASK NUMBER

5f. WORK UNIT NUMBER
664817.02.07.03.02

7. PERFORMING ORGANIZATION NAME(S) AND ADDRESS(ES)
NASA Langley Research Center
Hampton, Virginia 23681-2199

8. PERFORMING ORGANIZATION REPORT NUMBER

9. SPONSORING/MONITORING AGENCY NAME(S) AND ADDRESS(ES)
National Aeronautics and Space Administration
Washington, DC 20546-0001

10. SPONSOR/MONITOR'S ACRONYM(S)
NASA

11. SPONSOR/MONITOR'S REPORT NUMBER(S)
NASA/TM–2020–5004166

12. DISTRIBUTION/AVAILABILITY STATEMENT
Unclassified-Unlimited
Subject Category
Availability: NASA STI Program (757) 864-9658

13. SUPPLEMENTARY NOTES
An electronic version can be found at http://ntrs.nasa.gov.

14. ABSTRACT
Small unmanned aerial systems (UAS) are becoming increasingly common for private, military, and commercial use, increasing community noise exposure. Reducing the noise produced by UAS could help improve community acceptance. Active noise control (ANC) might be used to attenuate noise produced by UAS, however, traditional ANC systems require a physical sensor in the far-field, which is not feasible. This paper assesses a virtual error sensing (VES) method that eliminates the need for a far-field sensor. This paper describes the proposed VES strategy, and presents numerical simulations and experimental results that highlight the benefits and limitations of the approach. Results for the VES system alone and with an ANC approach are presented and discussed. Experimental testing focused on attenuating the tonal noise produced by one 2-bladed rotor with a tip radius of 11.9 cm. Pressure variations caused by blade rotation were measured in the near and far-field using electret microphones and externally polarized condenser microphones, respectively. The filtered-x least mean squares algorithm was used in conjunction with the VES system to attenuate the far-field response. Experimental results show reductions between 6-13 dB at varying far-field locations and rotation rates.

15. SUBJECT TERMS
UAS, rotor noise, active noise control, virtual error sensing

16. SECURITY CLASSIFICATION OF:			17. LIMITATION OF ABSTRACT	18. NUMBER OF PAGES	19a. NAME OF RESPONSIBLE PERSON
a. REPORT	b. ABSTRACT	c. THIS PAGE			STI Information Desk (help@sti.nasa.gov)
U	U	U	UU	24	19b. TELEPHONE NUMBER *(Include area code)* (757) 864-9658